

Preliminary Results of 5G Direction of Arrival Estimation using In-Situ Calibration with USRP

Alda Xhafa, Fran Fabra, José A. López-Salcedo and Gonzalo Seco-Granados

Universitat Autònoma de Barcelona (UAB), IEEC-CERES, Bellaterra, Spain

Abstract

The demand for high-precision location information in indoor positioning systems such as logistics, security, emergency etc., has increased the use of 5G systems as an alternative technology solution to the satellite-based positioning technologies. The 5G mobile networks provide more accurate and reliable positioning location in conditions of obstacles and changes. In this paper, the direction of arrival has been used for these localization approach. A description of In-Situ calibration of linear array antennas to enable direction of arrival estimation with 5G signals is provided. Despite the widely employed antenna arrays in 5G to facilitate the measurement of the direction of arrival (DOA), its performance is often degraded by array errors. Therefore, having coherent phases, accurate array manifold response, and delay and frequency offset OFDM waveform correction is a mandatory requirement to perform direction of arrival estimation. We provide an experimental validation of the calibration process and evaluate the DoA estimation performance using measurement data. In addition, we present a comparison among the performance of DoA estimation without calibration, when only the calibration of RF channel error is performed and when the full calibration including the antenna error calibration is done. It is then demonstrated via real test with commercial hardware equipment that an average reduction of 40% for DOA estimation error can be achieved by the proposed In-Situ calibration.

1. Introduction

In the recent years, with the rapid development of smart devices and technologies, there has been a strong demand on indoor Location-Based Services (LBS) [1] such as logistics, autonomous vehicles, localized sensing, as well as accurate indoor localization within buildings during emergency situations. Initially, the global navigation satellite systems (GNSS) have been the extensively used technology for LBS. Although these technologies can provide good location services, their performance is limited to the outdoor environment only. In indoor and in dense urban areas, the accuracy of the satellite-based positioning technologies degrades due to obstacles and environment changes by objects and multipath effects [2] in signal propagation. Therefore, the need for accurate and reliable location information has surge the use of 5G systems [3, 4, 5] as an effective solution for precise positioning, in concrete the direction of arrival (DOA) [6, 7] signal measurement.

The radio direction finding is closely related with the use of multiple antennas enabling high accuracy of position and orientation estimation, a strict requirement in the level of accuracy in 5G systems. An important prerequisite for antenna array base DoA estimation is phase coherence [9]. In practical systems, when dealing with radio-frequency front end hardware, the relative phase among receiver channels is object to severe degradation due to the system hardware and radio conditions. On the hardware side, the accuracy and stability of the radio front end phase synchronization depends on the drift in the clocks driving each RF chain,

WIPHAL 2023: Work-in-Progress in Hardware and Software for Location Computation, June 06–08, 2023, Castellon, Spain

✉ alda.xhafa@uab.cat (A. Xhafa); fabra@ieec.cat (F. Fabra); jose.salcedo@uab.cat (J. A. López-Salcedo); gonzalo.seco@uab.cat (G. Seco-Granados)

>ID 0000-0001-8724-3432 (A. Xhafa); 0000-0001-8100-1520 (F. Fabra); 0000-0002-5392-6005 (J. A. López-Salcedo); 0000-0003-2494-6872 (G. Seco-Granados)



© 2023 Copyright for this paper by its authors.

Use permitted under Creative Commons License Attribution 4.0 International (CC BY 4.0).

CEUR Workshop Proceedings (CEUR-WS.org)

manufacturing inaccuracies and temperature dependency. On the antenna side, the gain-phase, mutual coupling, antenna element position error, manufacturing imperfections may further contribute to the offset error. On the signal processing side, most of the algorithms for DoA estimation rely on a perfectly known antenna response restricted to an ideal antenna array. Any mismatch with the real antenna model [19] will deteriorate the DoA estimation performance. Moreover, the radio environment (i.e. multipath and interference) and misalignment in frequency and time domain can additionally constitute a significant source of DOA error. Therefore, to compensate the time varying phase offset as well as other gain and phase uncertainties due to the aforementioned limitations, a calibration process is needed to be carried out.

The calibration of antennas means that their antenna response is determined. The antenna calibration is mostly carried out in a controlled environment, i.e., without multipath propagation and interference, e.g., a dedicated measurement chamber. However, the antenna response is also affected by the surroundings. Therefore, it is important to measure the entire system, e.g., in a near-field measurements chamber, to obtain a better antenna response. This method can be costly. A more practical and less costly form to calibrate the antennas, is the In-Situ calibration method [13], where transmitters are used with a known direction to calibrate the antennas, but no propagation condition is known. The mutual coupling [12] and antenna element position error is introduced. However, this method is restricted to antenna arrays error models. In contrast to the previous method, the calibration of antennas is usually done performing the self-calibration that estimates the antenna parameters together with the DoA. This method attempts to avoid the calibration of antennas in a dedicated environment. However, it suffers from severe limitations from the lack of identification of antenna element and propagation conditions [14].

In this paper, we show the process of the In-Situ calibration of a linear array antenna of 4 elements to achieve high accuracy DoA estimation for the purpose of indoor positioning in conditions of multipath and interference effects. The sounding reference signal (SRS) for positioning in the uplink has been used for the estimation of angle of arrival, where an analytical model of time, frequency, and phase error of the array multichannel receiver has been done. The preliminary results of the 5G direction of arrival using the In-Situ calibration corrections has been presented followed by a discussion on the antenna response observability as well as DoA estimation performance and to showcase the advantage of using calibration error corrections.

2. System Model

In this work, an indoor DoA estimation scenario, where the uplink 5G signal is transmitted using an Universal Software Radio Peripheral (USRP) hardware N310 [8] from Ettus Research through one single channel node is considered. The selected transmitter has three master clock rates that allow a higher diversity in-sample rate, which makes it suitable when dealing with 5G signals where sampling rate and bandwidth are important. The transmitted signal through GNU Radio [16], an open-source software package, is received from a linear array antenna employed in a multichannel receiver. Since phase-coherence is very important in DoA estimation, a phase-coherent multichannel receiver, NI-2955 USRP [10] from National Instruments is selected. The channels should be synchronized in phase and time. This can be achieved through a configuration of Local Oscillators (LO) to enable the LO sharing capability of the receiver, limited to the USRP model.

2.1. Signal Model

We consider a 5G uplink reference signal (SRS) signal composed by 4 SRS symbols, each occupying M subcarriers, with M being the total number of subcarriers available for modulation. The subcarriers are symmetrically arranged around the central frequency. Note that, according

Table 1

Specifications of the uplink 5G signal considered in this work.

Parameter	Value
Nr. of antenna elements	4
Array model	ULA
Carrier frequency	2.4875 GHz
Subcarrier spacing	15 KHz
Nr. of subcarriers	2048
Pattern	Comb-two
Bandwidth	25 MHz
Sampling rate	30.72 MHz
Periodicity	every 1 ms

to 3GPP standard [15], 4 SRS symbols is the maximum that can be transmitted in one slot. The SRS is derived from the low peak-to-average power ratio (PAPR) Zadoff-Chu sequence whose entries are allocated at a specific time and frequency unit, also known as the physical resource unit, in the resource grid of the OFDM transmission scheme. Each entry of the Zadoff-Chu sequence will be allocated to physical resource unit in a resource block (RB) according to the parameters set following the configuration rules in 3GPP TS 38.211 [17]. The RB is the smallest logical block of the orthogonal frequency-division multiplexing (OFDM) grid, and it is composed of 12 subcarriers. The whole OFDM grid is composed of 14 OFDM symbols that constitutes one slot in time domain. Each Zadoff-Chu entry has been mapped to the corresponding resource element with a span of two subcarriers between two adjacent Zadoff-Chu sequence entries for each of the SRS symbols used. This is because, in frequency domain, the bandwidth for SRS can be adjusted and interleaving is permitted. The 5G NR also allows a swift arrangement of the RB used to allocate the SRS symbol and therefore the allocation bandwidth of the reference signal can be less than the total 5G bandwidth. In this work, a full-band SRS transmission has been used.

The subcarrier spacing is defined as $\Delta f = 1/T_s$, with T_s being the duration of the OFDM symbol without cyclic prefix (CP). CP is a repetition sequence of the last N_{cp} samples of the OFDM symbol that is placed at the beginning of the same symbol in order to prevent the inter-symbol interference from the previous OFDM symbol. The resource allocation pattern of the SRS signal used for transmission starts from the 11-th symbol until the 14-th symbol. Table 2 gives the configuration parameters to generate the uplink SRS signal.

Finally, the digital base-band of the i -th OFDM symbol in time-domain:

$$s_i[l] = \frac{1}{N_{fft}} \sum_{m=-\frac{N_{fft}}{2}}^{\frac{N_{fft}}{2}-1} S_i[m] \cdot e^{j \frac{2\pi}{N_{fft}} m(l-N_{cp})}, \quad (1)$$

with $l = 0, 1, \dots, N_{fft} + N_{cp} - 1$ being the sample index of an OFDM symbol, and m -th the OFDM subcarrier index, is generated using the IFFT. The digital signal s is transmitted by one source, periodically at a fixed repetition of time (with 4 SRS symbols per slot), at a predefined DoA and impinges on an antenna array of N elements. The received time-domain multichannel SRS signals are transformed to the frequency domain using FFT and removing the CP from each OFDM symbol. The stream at the n -th radio channel of the receiver is denoted as $\mathbf{x}_n = [X_{1,n}, X_{2,n}, \dots, X_{M,n}]^T \in \mathbb{C}^{M,1}$, where $X_{m,n}$ represents the received complex data SRS symbol at n -th receiving channel and m -th sub-carrier. The received signal at each received channel can be written also as:

$$X_{m,n} = a_n(\phi) s^n(l + \tau) \cdot e^{j\pi l \varepsilon} \cdot e^{j\Delta\Phi'_n} \cdot e^{j\hat{b}_n} + w_{m,n}, \quad (2)$$

where $a_n(\phi) = \sqrt{g_n(\phi)}e^{j\Phi_n(\phi)}$ is the antenna response at n -th front-end channel composed by the gain pattern $g_n(\phi)$ and phase pattern $\Phi_n(\phi)$, $s^n(l + \tau)$ is the delayed transmitted signal $s(n)$ received at n -th front-end channel, ε is the carrier frequency offset of the received signal at n -th front-end channel, $\Phi_n(\phi)$ is the phase offset introduced by the front-end hardware, and \hat{b}_n represent the rest of phase offset affecting in the error of antenna response such as antenna non-idealities including mutual coupling, manufacturing, as well imperfections and surrounding structure of the installation, multipath and/or interference. Lastly, w represents the noise at n -th receiving channel and m -th subcarrier. Each radio channel of the receiver represents a separated baseband received signal provided by the hardware front end. They are arranged into a single matrix $\mathbf{X} = [\mathbf{x}_1; \mathbf{x}_2; \dots; \mathbf{x}_N] \in \mathbb{C}^{M,N}$.

2.2. Phase-coherence Configuration

As previously stated, the array modeling errors that greatly depends on DoA estimation performance can be divided into two main error sources: one part induced by the antenna elements and the other part induced by the synchronization of channels in phase and time at the receiver side. The phase and amplitude imbalances between channels are needed to be corrected. Therefore, the multichannel receiver should be configured to enable the LO sharing between channels across multiple daughter-boards and eventually enabling the phase-aligned operation. There are several possible LO configurations that can be performed in NI-2955:

- *Independent*, where each channel will use its own LO and the LO input ports will be disabled.
- *Import*, where channels will use the LO provided at the corresponding import ports.
- *Shared and Export*, where channels will use the same LO from first channel, whose LO will be exported to their LO output ports.
- *Re-import*, where the LO from first channel is exported and both channels will use the LO provided at the corresponding import ports.
- *Shared*, where both channels of the same daughter-board will use the same LO from first channel of the channel couple.

In order to achieve coherent phases among the four channels, *LO-sharing* ability is enabled. One pair of channels is configured with *Shared and Export* and the other pair is set to *Import*. Then, the LO signal from the first pair is injected to the other pair with external cables through the corresponding LO ports. Another error source that effects in the phase alignment is the sampling rate. The received signals at all front ends should be sampled at the same time instant. NI-2955 provides a re-sampling process that allows to use a wide range of sampling rates. The USRPs include options for using an internal or external clock reference with the added ability to export the clock reference and time base. In this work, the receiver NI-2955 uses its internal clock giving a frequency accuracy of 2.5ppm.

3. In-Situ Calibration Process

The main focus in this work is to investigate the accuracy of DoA estimation in a realistic indoor environment, whose performance is influenced to a large extent by the calibration phase. The calibration procedure consists of three steps: RF channel error calibration; delay and carrier phase offset estimation and compensation of the received signal at each of n -th received channels; and antenna error calibration. All the calibration procedures involve placing the transmitter and the receiver hardware at a known distance and DoA, and performing repeated DoA measurements distributed over all possible directions limited to the sector coverage area of the environment, i.e., in the present case, -90° to 90° with an angular separation of 5° . All the measurements are conducted in an indoor working environment with line-of-sight

(LOS) propagation conditions. The transmitted waveform has been generated following the configuration parameters and conditions set by the 5G standard as explained in [15]. In the following subsections, details on each calibration process are provided. We mainly consider the imperfect array response from the antennas and the RF channel errors. These errors are compensated with RF channel coefficients that are pre-measured and calculated prior to calibration of the antenna's effect. Specific configuration of the hardware is needed to enable the phase coherence option.

3.1. RF Channel Error Calibration

The wideband 5G signal is conducted to the RF channels of the receiver by connecting all antenna ports of USRP-Rx NI-2955 via coaxial cables with a power splitter. The transmission of the 5G SRS signal is done through a single antenna port of USRP N310, at predefined system parameters: carrier frequency, sampling rate and transmission gain. The transmit power for this experiment is -15 dBm. On the receiver's side, each radio channel acquire the baseband stream provided by the hardware front-end at carrier frequency and sampling rate set in the transmission part and predefined reception gain; and store them in a custom binary data format with inphase/quadrature (I&Q) samples of 16 bits each. Both in transmission and reception, the transmission gain is set so that it avoids the distortion of the signal. The acquisition of the data stream of each radio channel is done in a sustained way for a predefined duration. The start and the end of the received OFDM signals define the phase of the waveform in the time domain. The phase difference between channels corresponds to the angle of the maximum peak of the cross correlation between one of the channels taken as reference with the rest of the channels. Because of the LO configuration explained in 2.2, all phases should be aligned.

The RF coefficients are measured by directly conducting the 5G uplink signal to the received RF channels. Since the LO configurations ensure the phase coherence during all time (even after a new power-cycle of the receiver maintaining the same system parameters), the differential phase-shift between the channel taken as reference and the rest of RF channels at the receiver's side is pre-measured before undergoing the calibration process of the antennas. These coefficients will be then compensated in both calibration and DoA estimation procedure. These coefficients are measured as the strongest correlation peak between the received waveform at the reference channel with the received waveform at the rest of the receiver RF channels. The calibration offsets are computed for every snapshot of the received data stream with duration of one slot and the average value of the computed coefficients is taken as a final calibration reference.

The USRP N310 has been deployed on a PC with an Intel i5-9500 CPU @ 3GHz and 32GB of RAM memory. The NI-2955 has been deployed on a PC with an Intel i7-10700 CPU @ 2.9GHz and 32GB of RAM memory. The latter has Windows 10 OS installed, while the other system has Ubuntu 22.04 LTS OS installed. The hard drives employed are Solid Stated Drives (SSD) NVMe-based of Category 3, enabling a sustained writing rate.

3.2. Time and Frequency offset estimation

The baseband I&Q samples are checked to estimate and establish the time and frequency synchronization to the uplink received signal with a local replica signal as a reference. Firstly, a coarse estimate of time and frequency offset is done in the time domain. No demodulation of the received waveform is performed to estimate the errors. Then a fine estimation and correction process is undertaken to refine the initial estimates and increase precision. This process synchronize the received data streams at each of the RF channels to the beginning of radio frame.

The initial carrier frequency offset (CFO) estimation is performed by the strongest correlation peak between the received waveform with the local replica of the signal. The CFO is estimated by making a search over a frequency range of residual carrier frequency to estimate, i.e. from

$-\Delta f$ to Δf with a step of one tenth of Δf that represents the value of the subcarrier spacing. For each of the frequencies in the search range, a compensation on the received signal is applied and a correlation of the corrected received signal $x[l]$ with a shifted and conjugated version of the reference signal $s[l]$ is computed. The resulting correlation is defined by

$$R_{rx}(l_\tau) = \sum_{l=0}^{M-1} x[l] \cdot s_c^*[l + l_\tau], \quad (3)$$

where $s_c[l]$ is a circular shifted of the local replica waveform resulting in a matched filter of the OFDM signal. The estimated delay can be expressed as

$$\hat{l}_\tau = \arg \max_{l_\tau} \{|R_{rx}(l_\tau)|^2\}, \quad (4)$$

where l_τ is the discrete time delay in samples. The process is repeated for each set of frequencies in the search range. The coarse time offset is chosen to be the one that gives the strongest correlation values and the corresponding correction frequency being the coarse frequency offset. Then, a data interpolation is performed in order to make a fine estimation of time and frequency offset around the coarse estimation value. The accuracy of the carrier frequency offset estimation is limited to the subcarrier spacing.

3.3. Antenna error calibration

Apart from the RF channel errors induced by the multichannel receiver, the effect of the mutual coupling between antenna elements, the location perturbations and beam-pattern errors of antenna elements, as well as other radio conditions, the antenna errors are direction-dependent. The estimation of DoA is done evaluating the phase offsets across receiving antennas. The receiving array elements (an uniform linear array (ULA) with a half-wavelength spacing) are swiveled within a specified sector coverage and a predefined angular step. For each of the known DoA to estimate, after RF channel error, and time and frequency offset correction, the phase offsets caused by free-space propagation are evaluated and compensated to the received data stream. The channel response of array antenna at the receiver side is used to estimate the actual array manifold and compared with the true manifold $\mathbf{a}(\phi)$. The mismatch between manifolds (i.e., deviation of the actual manifold from the ideal one) will serve as a reference metric for correcting the array response during the DoA estimation. The calibrated array manifold $\hat{\mathbf{a}}(\phi)$ aims to delineate the true array response with the array error computed and corrected in the searching-based DoA estimation algorithms. The searching-based DoA estimation algorithm, in concrete the multiple signal classification method (MUSIC), can directly employ this calibrated array manifold. The calibrated array manifold can be expressed as

$$\hat{\mathbf{a}}(\phi) = \text{diag}(\zeta(\phi)) \cdot \mathbf{a}(\phi), \quad (5)$$

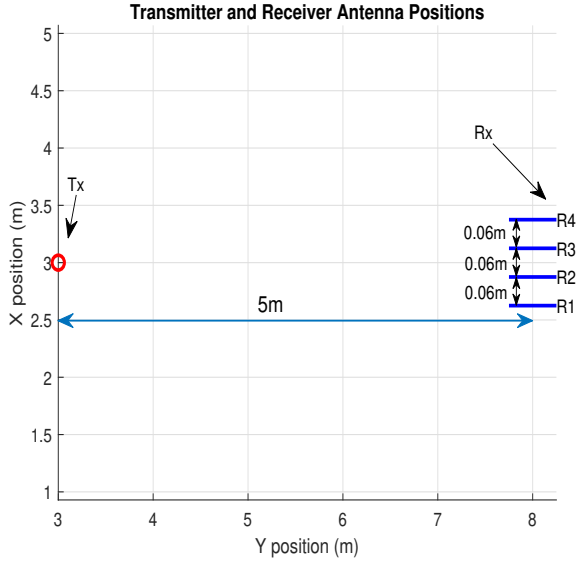
with $\zeta(\phi) = [1, e^{j\hat{b}_2}, \dots, e^{j\hat{b}_N}]$ being the mismatch array error correction obtained from the In-Situ calibration process and $\mathbf{a}(\phi) = [1, e^{\frac{-j2\pi d \sin(\phi)}{\lambda}}, \dots, e^{\frac{-j2\pi(N-1)d \sin(\phi)}{\lambda}}]$ being the theoretical antenna response where d is the antenna element distance. Then, dominant spectral peaks are used to find the DoAs.

4. Experimentation set-up

The calibration process has been conducted in an 56 m^2 empty laboratory room of the office building, where a single transmitter and receiver are placed within a distance of 5 m (see 1(a) and 1(b)). A sector of 180° , i.e., -90° to 90° with an angular step of 5° corresponding to 37



(a) Environmental Layout



(b) Experimental Setup

Figure 1: Set-ups for In-Situ calibration and DoA estimation experiments in a 56 m^2 room size. The X and Y positions in 1(b) correspond to the width and length room size respectively. The receiver is placed near to the wall at one extreme of the room length and the transmitter is placed 3 m away from the other extreme of the room length (see 1(a), 1(b)). The Tx and Rx are placed within a distance of 5m and each antenna element on the receiver side has a spacing of 0.0603 m in between.

pilot angles of arrival evenly distributed is considered. Note that the sector coverage is limited by the scenario where the experiments are performed. The receiver is placed near the wall, at one side of the room and the transmitter is placed 3 m away from the other side as in 1(b). To obtain different DoA, the array manifold at the receiver side is swiveled. The SRS signal is transmitted periodically every 1 millisecond during 2 sec from the single antenna port of USRP-Tx N310. The system parameters used are a carrier frequency of 2.4875 GHz, transmission gain of 65 dB, and sampling rate of 30.72 Msps, corresponding to 25 MHz bandwidth with Fast Fourier Transform (FFT) length 2048. Both the transmitter and receiver utilize the same antenna modules, omnidirectional monopole antennas. The single transmitter antenna is mounted directly on one of the transmission channels of USRP-Tx N310, while on the receiver's side the antennas are mounted in a platform with a separation of $\lambda/2$ between elements of the antenna. Two sets of measurements for each of the pilot angles of arrival are taken. The first set of data stream will serve to perform calibration of the antenna errors and the other set will be used to evaluate the performance of DoA estimation under the conditions of calibration and non calibration. The phase offsets between antennas are computed by averaging over phases of subcarriers with the same carrier frequency. All experiments are carried out under LOS condition.

Because an ISM radio band is used for transmission, the presence of interference is inevitable. During the experimentation process, the presence of a signal at center frequency of 2.479 GHz of 2 MHz bandwidth has been detected. To improve the resolution ability, interference correction is undertaken by choosing only the subcarriers that does not contain the interference after the demodulation of the waveform.

Table 2
DoA estimation performance

Calibration Method		No calibration	RF channel calibration	RF channel & antenna error calibration
rmse_DoA_estimate (°)	max	151.64	58.16	3.35
	min	5.9	0.07	0.007
std_estimation_error (°)	max	17.32	14.58	0.58
	min	0.04	0.02	0.003

5. Experimental results

The experiments have been conducted twice: one to compute the mismatching between ideal array manifold response, and the other to investigate the impact of calibration in DoA estimation, as well as the impact of the multipath condition in the estimation accuracy. Figure 2 shows the theoretical array response for each of the incident direction; the corresponding experimental array response and the estimated array phase error from the expected value. The latter will serve as a mismatch parameter to correct the phase error coming from the antennas. These results are computed after correcting the phase offset between channels coming from the RF channels. Results show that, even in conditions of multipath and interference, the computed steering vector follows the behavior of the theoretical one that considers an ideal antenna response. Note that the interference is eliminated by excluding the subcarriers that contain the interference signal.

The presence of multipath effects in the propagation delay of a reference signal at each m -th subcarrier of the signal has a phase shift of $\sum_{k=1}^K \alpha^k \cdot e^{-j2\pi m \Delta f \tau^k}$, with τ^k being the propagation delay of k -path, K being the total number of paths of the propagation channel and α^k being the absolute amplitude of the k -th signal. In severe multipath conditions, the effect of propagation delay for each of the subcarriers is 5.3° within successive subcarriers. For the incident angles in between the angles, at which the tests are performed, an interpolation within the range of array modeling errors set of data (computed during antenna error calibration process) is done. All these inaccuracies depend on the performance of the DoA estimation, reflected in the results shown in Figure 3. Results show a significant improvement in DoA estimation accuracy with a maximum of 46.74% when applying only the RF channel error corrections. The large improvement in the accuracy of DoA estimation show the high phase offset that the received RF channels apply and therefore a severe degradation on the angle of arrival is faced. Moreover, an additional reduction of error estimation of maximum 25.9% is noted when the antenna error correction is applied, especially in cases close to the end-fire array where unsatisfactory performance is expected. The maximum error estimation deviation reaches ± 17.32 degrees and it reduces up to less than one degree (± 0.58) when applying the full calibration corrections estimated during In-Situ calibration. These results show the importance of the calibration process enabling the stability and accuracy of the DoA estimation since the measured antenna array manifold severely deviates from the nominal manifold. Therefore, the In-Situ measurements cause improvement of the incident angles as it captures the real array responses more precisely by using the post-established in-field measurements.

All in all, the preliminary results show that with only calibrating the received RF channels, a significant improvement is achieved. A precise estimation is achieved when the antenna errors are also considered in the DoA estimation process.

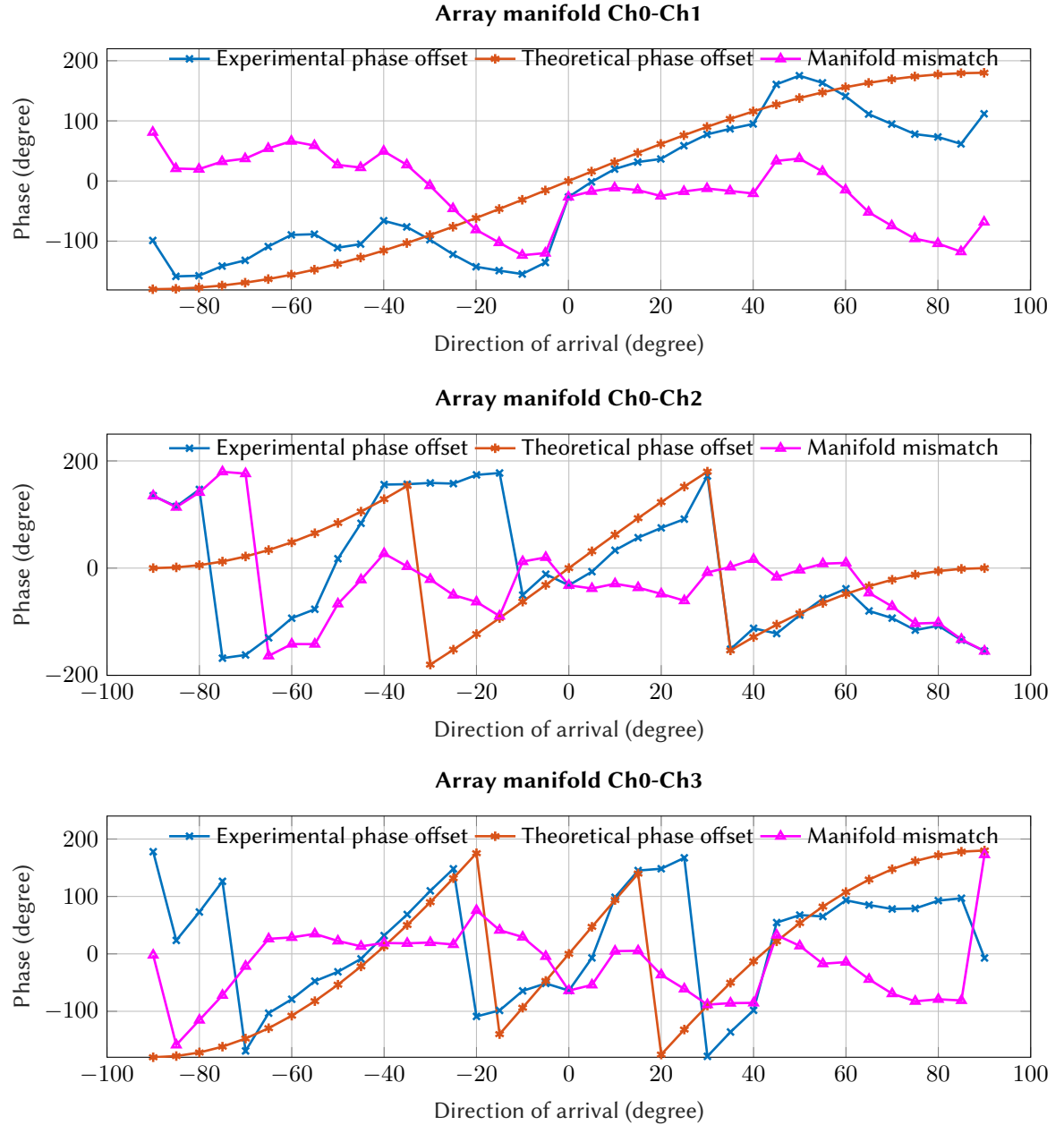


Figure 2: Antenna phase errors at pilot direction of arrival.

6. Conclusions

In this work we presented the preliminary results of 5G DoA estimation using In-Situ calibration metric for the purpose of accurate indoor positioning solution even in conditions of multipath and interference in signal propagation. Moreover, the required steps to achieve coherent phases between RF channel of a universal radio receiver are presented. The obtained results show a significant improvement of DoA estimation accuracy because of calibration. The calibration process fully exploits the bandwidth resources provided by 5G signal to resolve the presence of interference in the measurement data. We believe this is an important step to provide high precision DoA estimation and therefore an accurate positioning location. Moreover, it is shown a scalable solution to calibrate universal hardware and antenna arrays.

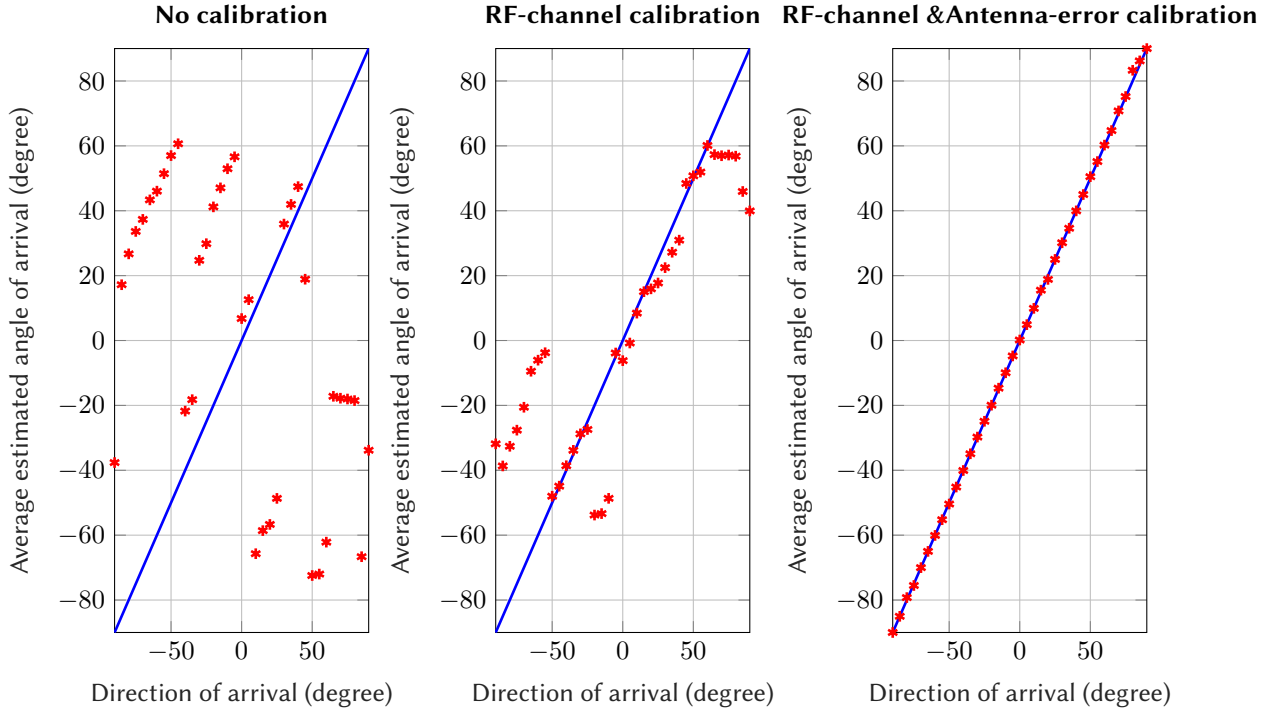


Figure 3: Estimation angle of arrival accuracy.

Acknowledgments

This work was supported in part by the Spanish Agency of Research (AEI) under the Research and Development projects PID2020-118984GB-I00/AEI/10.13039/501100011033 and PDC2021-121362-I00/AEI/10.13039/501100011033; and mobility grant SEBAP (Societat Económica Barcelonesa d'Amics del País).

References

- [1] N. El-Sheimy and Y. Li, "Indoor navigation: State of the art and future trends," *Satell. Navig.*, vol. 2, art. no. 7, pp. 1–23, May 2021.
- [2] J. A. del Peral-Rosado, J. A. López-Salcedo, G. Seco-Granados, F. Zanier and M. Crisci, "Evaluation of the LTE positioning capabilities under typical multipath channels," 2012 6th Advanced Satellite Multimedia Systems Conference (ASMS) and 12th Signal Processing for Space Communications Workshop (SPSC), Vigo, Spain, 2012, pp. 139–146, doi: 10.1109/ASMS-SPSC.2012.6333065.
- [3] B. Sun, B. Tan, W. Wang, and E. S. Lohan, "A comparative study of 3D UE positioning in 5G new radio with a single station," *Sensors*, vol. 21, no. 4, p. 1178, Feb. 2021.
- [4] M. Koivisto, M. Costa, J. Werner, K. Heiska, J. Talvitie, K. Leppanen, V. Koivunen, and M. Valkama, "Joint device positioning and clock synchronization in 5G ultra-dense networks," *IEEE Trans. Wireless Commun.*, vol. 16, no. 5, pp. 2866–2881, May 2017.
- [5] E. Y. Menta, N. Malm, R. Jantti, K. Ruttik, M. Costa, and K. Leppanen, "On the performance of AoA-based localization in 5G ultra-dense networks," *IEEE Access*, vol. 7, pp. 33 870–33 880, Mar. 2019.
- [6] M. Hua, C. Hsu, W. Liao, C. Yao, T. Yeh, and H. Liu, "Direction-of-Arrival Estimator using Array Switching on Software Defined Radio Platform," in 2011 IEEE International Symposium on Antennas and Propagation (APSURSI), July 2011, pp. 2821–2824.

- [7] M.-C. Hua, C.-H. Hsu, and H.-C. Liu, "Implementation of Direction-of-Arrival Estimator on Software Defined Radio Platform," in 2012 8th International Symposium on Communication Systems, Networks Digital Signal Processing (CSNDSP), July 2012, pp. 1–4.K.
- [8] Ettus. Ettus Research Knowledge Base: USRP N300/N310. Available: <https://kb.ettus.com/N300/N310>.
- [9] Pohlmann, R., Zhang, S., Staudinger, E., Caizzone, S., Dammann, A., & Hoeher, P. A. (2022). Bayesian In-Situ Calibration of Multiport Antennas for DoA Estimation: Theory and Measurements. *IEEE Access*, 10, 37967–37983. <https://doi.org/10.1109/access.2022.3164520>.
- [10] Product documentation-NI. NI2955. <https://www.ni.com/docs/de-DE/bundle/usrp-2955-specs/page/specs.html>.
- [11] Z.-M. Liu and Y.-Y. Zhou, "A unified framework and sparse Bayesian perspective for direction-of-arrival estimation in the presence of array imperfections," *IEEE Trans. Signal Process.*, vol. 61, no. 15, pp. 3786–3798, Aug. 2013.
- [12] Y. Wang, L. Wang, J. Xie, M. Trinkle, and B. W.-H. Ng, "DOA estimation under mutual coupling of uniform linear arrays using sparse reconstruction," *IEEE Wireless Commun. Lett.*, vol. 8, no. 4, pp. 1004–1007, Aug. 2019.
- [13] I. Gupta, J. Baxter, S. Ellingson, H.-G. Park, H. S. Oh, and M. G. Kyeong, "An experimental study of antenna array calibration," *IEEE Trans. Antennas Propag.*, vol. 51, no. 3, pp. 664–667, Mar. 2003.
- [14] P. Heidenreich and A. M. Zoubir, "High-resolution direction finding of coherent sources in the presence of model errors using alternating projections," in 2009 IEEE/SP 15th Workshop on Statist. Signal Process., Cardiff, UK, Aug. 2009, pp. 521–524.
- [15] 3GPP, "Study on NR positioning enhancements (Release 17)," <http://www.3gpp.org/DynaReport/38857.htm>, 3rd Generation Partnership Project
- [16] Usage Manual - GNU Radio. https://wiki.gnuradio.org/index.php/Usage_Manual. Project (3GPP), Technical Report (TR) 38.857, Mar. 2021.
- [17] 3GPP, "NR; Physical channels and modulation," <http://www.3gpp.org/DynaReport/38211.htm>, 3rd Generation Partnership Project (3GPP), Technical Specification (TS) 38.211, Jun. 2021.
- [18] De Angelis, Guido & Angelis, Alessio & Händel, Peter & Carbone, Paolo. (2010). Estimation of the Calibration Parameters for an UWB Indoor Positioning System.
- [19] Eberhardt, Michael & Eschlwech, Philipp & Biebl, Erwin. (2016). Investigations on antenna array calibration algorithms for directionofarrival estimation. *Advances in Radio Science*. 14. 181190. 10.5194/ars141812016.